Paper No. 36

THERMO-MECHANICAL ANALYSES OF DYNAMICALLY LOADED RUBBER CYLINDERS

Arthur R. Johnson* and Tzi-Kang Chen
Army Research Laboratory, MS 240
Analytical and Computational Methods Branch
NASA Langley Research Center
Hampton, VA 23681-2199

Presented at a meeting of the

Rubber Division, American Chemical Society

Pittsburgh, PA

October 8-11, 2002

*Speaker

THERMO-MECHANICAL ANALYSES OF DYNAMICALLY LOADED RUBBER CYLINDERS[1]

Arthur R. Johnson and Tzi-Kang Chen
Army Research Laboratory, MS 240
Analytical and Computational Methods Branch
NASA Langley Research Center
Hampton, VA 23681-0001

ABSTRACT

Thick rubber components are employed by the Army to carry large loads. In tanks, rubber covers road wheels and track systems to protect roadways. It is difficult for design engineers to simulate the details of the hysteretic heating for large strain viscoelastic deformations. In this study, an approximation to the viscoelastic energy dissipated per unit time is investigated for use in estimating mechanically induced viscoelastic heating. Coupled thermo-mechanical simulations of large cyclic deformations of rubber cylinders are presented. The cylinders are first compressed axially and then cyclically loaded about the compressed state. Details of the algorithm and some computational issues are discussed. The coupled analyses are conducted for tall and short rubber cylinders both with and without imbedded metal disks.

INTRODUCTION

Rubber is employed to carry large loads in tires, gaskets, and tank track pads. It is also used to provide damping and system stability in complex mechanical systems such as helicopter rotors. In these applications, the rubber is typically stiffened by the addition of carbon black. The filled rubber tends to be a poor conductor of heat, yet it also exhibits very large hysteretic energy loss during cyclic loading. Also, the mechanical properties of rubber are strongly dependent on temperature. Faced with the above issues, designers interested in modeling the detailed response of complex-shaped rubber components need to be able to compute the coupled thermo-mechanical behavior of rubber.

An example of the importance of understanding the thermo-mechanical response of filled rubber is given in a series of papers presented at the "Thirty Second Sagamore Army Materials Research Conference" held a Lake Luzerne, NY in 1985.[1-4] In these papers, hysteretic heating, thermo-mechanical degradation, and fatigue of rubber-coated road wheels and tank track pads are all discussed. Uncoupled thermo-mechanical finite element analyses, and sensitivity studies were conducted with finite element codes. It was observed that the viscoelastic properties and the shape of the rubber solid are the most important factors in determining temperature rise.[1] The degradation studies indicate that the failure of cyclically loaded "rubber-like" polyurethane blocks depends on the hard segment transition temperature.[2] Experiments were conducted which

[1]This paper is declared a work of the U.S. Government and is not subject to copyright protection in the United States.

proved that the large strain hysteretic heating rate does not correlate with the heating rates predicted using the popular complex modulus material data.[3] Also determined is the fact that failure under cyclic loading can be "significantly different from that obtained in constant strain rate testing."[4] These conclusions suggest that detailed computational simulations of large strain dynamic loading of rubber-like solids, performed as part of a material degradation study, require accurate modeling of the large strain viscoelastic properties and a coupling of the mechanical and thermal models.

In this paper, large deformation rubber viscoelasticity and heat transfer finite element models are coupled and employed to simulate the hysteretic heating of dynamically loaded rubber cylinders. The purpose of the work is to establish and test a computational tool for analyzing hysteretic heating in rubber components.

The formulations for large strain rubber viscoelasticity and heat transfer employed in ABAQUS are outlined below to facilitate the description of the thermo-mechanical coupling performed in this study. Detailed information on these two formulations and their finite element implementation is available in the ABAQUS Theory Manual.[5] Additional information on formulations for rubber viscoelasticity is available in the literature.[6-10] Only moderate temperature changes were simulated in this study, so time-temperature superposition is not discussed.

RUBBER ELASTICITY

The coordinates of a material point in the reference configuration are indicated by $\mathbf{X} = \{X_1, X_2, X_3\}$ and in the deformed configuration by $\mathbf{x} = \{x_1, x_2, x_3\}$. The vector function $\mathbf{x} = \mathbf{x}(\mathbf{X}, t)$ defines the mapping of points from the reference configuration into the deformed configuration. The Lagrangian method is employed to describe the deformed solid's energy. The matematical tools employed are listed in the APPENDIX. The virtual work statement, excluding inertial effects, for a deformed solid of volume V and surface area S is

$$\delta W_I = \int_V \mathbf{s} : \delta \mathbf{D}_{\mathrm{v}} \, dV = \int_S \delta \mathbf{v}^T \mathbf{t} \, dS + \int_V \delta \mathbf{v}^T \mathbf{f} \, dV \tag{1}$$

where $\delta \mathbf{v}$ is a virtual displacement vector, δW_I is the internal energy due to the virtual displacement, $\delta \mathbf{D}_{\mathrm{v}}$ is the virtual rate of deformation, $\mathbf{t}$ is the traction stress prescribed over S, and $\mathbf{f}$ is the body force vector acting within the volume V, and V_0 is the volume in the undeformed state. When the solid is rubber, the internal energy in Equation (1) is expressed as follows.

$$\delta W_I = \int_{V_0} \left\{ 2 \left[\left(\frac{\partial U}{\partial \bar{I}_1} + \bar{I}_1 \frac{\partial U}{\partial \bar{I}_2} \right) \overline{\mathbf{B}} - \frac{\partial U}{\partial \bar{I}_2} \overline{\mathbf{B}}^2 \right] : \delta \mathbf{e} + J \frac{\partial U}{\partial J} \, \delta \varepsilon^{vol} \right\} dV_0 \tag{2}$$

where U is the strain energy density function defined in this effort as

$$U = \frac{G_0}{2}\left(\bar{I}_1 - 3\right) + \frac{k_0}{2}\left(J-1\right)^2 \tag{3}$$

where G_0 is the instantaneous shear modulus and k_0 is the instantaneous bulk modulus.

RUBBER VISCOELASTICITY

The present analysis employs the large strain viscoelasticity model adopted in ABAQUS.[5] The model assumes that stress relaxation can be described by a Prony series. The shear and bulk moduli are expressed in the form

$$G(t) = G_\infty + \sum_{i=1}^{N} G_i\, e^{\frac{-t}{\tau_i}} \qquad \text{and} \qquad K(t) = K_\infty + \sum_{i=1}^{N} K_i\, e^{\frac{-t}{\tau_i}} \tag{4}$$

where $G_0 = G(t=0)$, $K_0 = K(t=0)$, and τ_i denote relaxation time constants. The constitutive model employed is a BKZ-like model in which the deviatoric, $\mathbf{s}^D$, and hydrostatic, $\mathbf{s}^H$, stresses are determined as follows.

$$\mathbf{s}^D(t) = \mathbf{s}_0^D(t) - SYM\left[\sum_{i=1}^{N} \frac{g_i}{\tau_i} \int_{\xi=0}^{t} \mathbf{F}_t^{-1}(t-\xi)\mathbf{s}_0^D(t-\xi)\mathbf{F}_t(t-\xi) e^{\frac{-\xi}{\tau_i}}\, d\xi\right] \tag{5}$$

and

$$\mathbf{s}^H(t) = \mathbf{s}_0^H(t) - \sum_{i=1}^{N} \frac{k_i}{\tau_i} \int_{\xi=0}^{t} \mathbf{s}_0^H(t-\xi) e^{\frac{-\xi}{\tau_i}}\, d\xi \tag{6}$$

where $g_i = G_i / G_0$, $k_i = K_i / K_0$, and $\mathbf{F}_t(t-\xi)$ is the deformation gradient of the deformed shape at time $t-\xi$ relative to the deformed shape at time t. Approximations are made when Equations (5) and (6) are integrated so that the entire history does not have to be convoluted. The approximations depend on the material constants being of Prony series form. Throughout the remainder of this paper only one term in the Prony series will be employed and the Prony series subscripts will be dropped.

HEAT TRANSFER

The variational statement of the energy balance equation for heat transfer, together with Fourier's law, for a deformed solid of volume V, and surface area S is:

$$\int_V \rho \frac{dU_\theta}{dt} \delta\theta \, dV + \int_V \frac{\partial \delta\theta}{\partial \mathbf{x}} \mathbf{k} \frac{\partial \theta}{\partial \mathbf{x}} \, dV = \int_V \delta\theta \, r \, dV + \int_S \delta\theta \, q \, dS \tag{7}$$

where θ is the temperature, U_θ is the internal thermal energy, ρ is the mass density, q is the heat flux per unit area, r is the heat supplied per unit volume, $\mathbf{k}$ is a conductivity matrix, and

$\delta\theta$ is a virtual temperature field satisfying the essential boundary conditions. Equation (7) is used to build the transient heat transfer finite element equations for the rubber solid.

Finite element discretization of the mechanical and thermal variational statements, Equations (1) and (7), results in systems of time dependent differential equations which approximate the mechanical and thermal response of the solid. It is difficult to compute the viscoelastic energy dissipated per unit time for the constitutive model described above. This mechanically generated energy dissipation is required if one needs to couple the mechanical and thermal analyses. Below we investigate approximating the energy dissipation with a simple formula involving the viscous components of stress. The formula is of the same form as the dissipation formula for a Maxwell model.

ANALYTICAL

The mathematical relation for computing the energy dissipation per unit time for a constitutive model in history integral form involves a double convolution integral in time.[11] To avoid such a difficult computation we exploit the fact that when the relaxation modulus is in Prony series form, the convolution integral in the BKZ-like constitutive model can be approximated with a finite difference equation that is similar in form to the finite difference equation for a Maxwell solid. This suggests that we explore the use of the Maxwell solid's dissipation function (which is easily computed) for approximating mechanically induced heating in a BKZ-like viscoelastic solid.

FINITE DIFFERENCE EQUATIONS FOR VISCOUS STRESS COMPONENTS

A simplified one-dimensional version of the finite difference equations (across a time interval $\Delta t = t_{n+1} - t_n$) for the evolution of the viscous stress, σ^v, that is valid for the BKZ-like model described above is given by[5]

$$\sigma^v_{n+1} = \left\{ \left(1 - \frac{\tau}{\Delta t}\left(1 - e^{\frac{-\Delta t}{\tau}} \right) \right) \hat{\sigma}^0_{n+1} + \left(\frac{\tau}{\Delta t}\left(1 - e^{\frac{-\Delta t}{\tau}} \right) \right) \hat{\sigma}^0_n \right\} g + e^{\frac{-\Delta t}{\tau}} \sigma^v_n \tag{8}$$

where $\hat{\sigma}^0_k$ is a viscous stress increment computed at time t_k using the relative deformation gradient between configurations at times t_{k-1} and t_k, and using the instantaneous modulus, G_0, of the material. The analogous finite difference equation for the viscous component of stress in a Maxwell solid (obtained by employing the trapezoidal method) is given by

$$\sigma^v_{n+1} = \left\{ \frac{\sigma^0_{n+1} - \sigma^0_n}{\left(1 + \frac{\Delta t}{2\tau} \right)} \right\} g + e^{\frac{-\Delta t}{\tau}} \sigma^v_n \tag{9}$$

where $\left(\sigma^{0}_{n+1} - \sigma^{0}_{n}\right)$ is a stress increment computed using the total strain (i.e., current configuration's strain) and using the instantaneous modulus of the material.

For a time interval in which the stress increment terms, $\{\bullet\bullet\bullet\}g$, in Equations (8) and (9) are approximately equal, or in which the stress increment terms have small values relative to the stress decay term, $e^{\frac{-\Delta t}{\tau}}\,\sigma^{v}_{n}$, the Maxwell model and the BKZ-like model will have stress histories that are approximately equal. This implies that the dissipation functions will also be approximately equal.

DISSIPATION FUNCTION

A deformation suddenly imposed at time $t = 0$ and which is subsequently maintained constant, produces stress relaxation. When the rubber's relaxation shear modulus is of Prony series form the energy dissipation per unit volume, $r(t)$, during relaxation is of the form

$$r(t) = \frac{dU^{v}_{s}}{dt} = \frac{-U^{v}_{s}\left(t = 0^{+}\right)}{\tau} \tag{10}$$

where $U^{v}_{s}\left(t = 0^{+}\right)$ is the viscoelastic shear energy density which results from the sudden deformation. Note, the rubber solid is incompressible in this study and there is no dissipation from the volumetric viscous stresses. In the case of a Maxwell solid, the dissipation per unit volume, $r_{Max}(t)$, during a time dependent process is of the form

$$r_{Max}(t) = \frac{-2\,U^{v}_{s}(t)}{\tau} \tag{11}$$

where $U^{v}_{s}(t)$ is the viscoelastic shear energy density in the Maxwell solid's spring-dashpot leg. Since the finite difference stress evolution equations in the finite element code used here (ABAQUS) are similar in form to Maxwell solid equations, we selected to employ the dissipation function in Equation (11), for estimating hysteretic heating from large strain viscoelastic deformations. Values of $U^{v}_{s}(t)$ were approximated by assuming the current value of the viscous stress, $\mathbf{s}^{v}(t)$, is derived from a linear internal solid in a Maxwell link which has a time constant given by τ. The resulting dissipation function is given by

$$r(t) = \frac{\mathbf{s}^{v} : \mathbf{s}^{v}}{2\,g\,G_{0}\,\tau} \geq 0 \tag{12}$$

where $g\,G_{0}$ is the viscous shear modulus.

FINITE ELEMENT EMPLOYED

The ABAQUS finite element code was employed to perform the calculations. The code allowed us to run the mechanical and thermal algorithms simultaneously in time and to exchange data between the algorithms. We present the details for the 2D axisymmetric model (the procedure is similar for the 3D solid model.)

The eight-node hybrid axisymmetric CAX8RHT element was used, see Figure 1. The interpolation is biquadratic for the displacement field, and bilinear for the temperature and pressure fields. Reduced integration is also employed. The nodal variables employed in the thermal element to describe the interpolation are the temperatures, θ, at the four corner nodes. The stress element has radial, u_r, and axial, u_z, displacements at the eight nodes and hydrostatic pressure, p_i, variables at each of the four integration points. The heating rates, $r(t)$, are applied at the four integration points.

HYSTERETIC HEATING IN RUBBER CYLINDERS

To investigate the application of the procedure described above, four cylinders were analyzed for hysteretic heating. Only moderate temperature changes were simulated so the elastic material constants were not treated as temperature dependent. Having the elastic constants independent of temperature simplified the calculations presented in this effort, but it is not a limitation of the algorithm.

CYLINDER DIMENSIONS AND MATERIAL PROPERTIES

There were two groups of two cylinders each. One group consisted of uniform cylinders and the other group had steel disks at their centers, see Figure 2. All cylinders had the radius, $R = 0.0282\,m$. There were two cylinder heights in each group. The heights were $H = 0.05\,m$, and $0.0125\,m$ respectively. The cylinders were compressed between steel fixtures. The model simulates the case when a lubricant maintains the fixture-rubber interface as frictionless. The internal steel disks were completely attached (bonded) to the rubber. The height and radius of the disks were $0.0025\,m$, and $0.0141\,m$ respectively.

The rubber energy density was modeled as a Neo-Hookean solid (Equation (3)). The viscous behavior was described with one Prony term (Equation (4)). The material constants employed are representative of a filled rubber and are listed below.[12-15] The viscoelastic constants for the rubber are $G_0 = 2.310\,MPa$, $\mathrm{k}_0 = \mathrm{k}_\infty = 2.000 * 10^3\,MPa$, $g = 0.3$, $k = 0.0\,MPa$, and $\tau = 0.1\,\mathrm{s}$. The elastic constants for the steel are Young's modulus $E = 206.8\ G\,Pa$ and Poisson's Ratio $\nu = 0.3$. The film heat transfer coefficients for the rubber-air and rubber-steel interfaces are $h_A = 5.44284 J/\left(^\circ C\,m\,\mathrm{s}\right)$ and $h_S = 20934\,J/\left(^\circ C\,m\,\mathrm{s}\right)$, respectively. The remaining thermal material constants are shown in Table I.

PRESCRIBED AXIAL DISPLACEMENT AND RESULTS

The deformation of the tall ($H = 0.05\,m$) uniform cylinder subjected to an axial displacement is shown in Figure 3. Since the boundary conditions are symmetric, only the half height (r, z)-quadrant is shown. The mesh refinement near the top and outer edges is to accommodate the heat transfer gradients at those locations. Each cylinder was subjected to an axial enforced displacement that produced large strain hysteresis. The half height enforced axial displacement for the tall cylinder is described as follows. The top end of the cylinder was ramped to a displacement of $-0.0045\,m$ in $0.05\,s$. The top end of the cylinder was then forced to follow the prescribed axial displacement given by

$$u_z(t) = -0.0045 - 0.003\,\sin(40.84\,t)\;m \tag{13}$$

The half height enforced axial displacement for the short cylinder is described as follows. The top end of the cylinder was ramped to a displacement of $-0.001125\,m$ in $0.05\,s$. The top end of the cylinder was then forced to follow the prescribed axial displacement given by

$$u_z(t) = -0.001125 - 0.00075\,\sin(40.84\,t)\;m \tag{14}$$

where t is the time in seconds. The loading and the displacement of the top of the cylinder are shown in Figure 4 for a time interval of 1.0 s. As expected, the displacement curve demonstrates viscoelastic softening. A number of analyses were performed to test the nonlinear elastic, the viscoelastic, and the transient heat transfer finite element algorithms separately. Hand calculations and finite difference calculations verified that the algorithms functioned correctly. The thermal boundary conditions did not significantly affect the temperature fields computed. The following analyses were performed, employing the dissipation function described above, to investigate the non-uniform heating of rubber cylinders undergoing large strain dynamic deformations.

Uniform Cylinders. The cyclic deformations given by Equations (13) and (14) were applied to the tall and short uniform cylinders indicated by the dimensions given above. The temperatures, at the center of the cylinders, $(r = 0, z = 0)$, as a function of time for the first 20 s of loading are shown in Figure 5. The frictionless rubber-fixture boundary condition allows the strains to be uniform in the cylinder. Rubber is a poor conductor of heat and the fact that the cylinders heated nearly uniformly regardless of height was expected.

Cylinders with Imbedded Disks. It is difficult to estimate hysteretic heating in rubber solids of complex shape because coupled thermo-mechanical analyses are needed in regions of high strain gradients. Tall and short cylinders with imbedded steel disks were cyclically loaded to simulate the distribution of viscoelastic heating in a rubber solid when the deformations produce high strain gradients. The results obtained appear reasonable. Figure 6 shows the meshes on the reference and deformed shapes for the tall cylinder. The temperature distribution in the tall block after 20 s of dynamic loading is shown in Figure 7. Temperatures at points A, B, C, and D in Figure 7 are plotted as a function of time in Figure 8. The outer radial end of the internal disk (point C) is predicted to heat much faster than the rest of the cylinder.

Similar results were obtained for the short cylinders. However, there were some convergence problems that were overcome by re-meshing near the top outer corner of the steel insert and employing lower order displacement interpolations (the four node displacement element was employed.) The temperature distribution in the short cylinder is shown in Figure 9. Again, Figure 10 shows that the region of high strain gradient, located near the outer radial end of the internal disk (point C), has the most rapid rise in temperature.

SUMMARY

Accurate predictions of the strain and temperature distributions in rubber components, employed in dynamically loaded structures, are required to perform degradation studies. A procedure that couples a viscoelastic large dformation stress analysis with a heat transfer analysis was described with the use of the ABAQUS finite element code. A user subroutine was written to approximate the time rate of energy dissipation per unit volume and to pass this data from the stress routine to the heat transfer routine.

The thermo-mechanical heating of tall and short uniform rubber cylinders (without internal disks) was computed using the coupling procedure. The viscoelastic material properties employed are valid for large strain deformations of rubber. The time dependent strains in the cylinders were uniform, and uniform heating was computed. The thermo-mechanical heating of tall and short rubber cylinders, containing internal steel disks, was also computed. The internal steel disks provided high strain gradients within the rubber cylinders and nonuniform hysteretic heating was observed. The analyses performed suggest that the coupling procedure should be considered for further development as a design tool for rubber degradation studies.

REFERENCES

[1]D. R. Lesuer, A. Goldberg, and J. Patt, "Elastomers and Rubber Technology," Eds. R. E. Singler and C. A. Byrne, Library of Congress 86-600600, pp. 211 - 228.

[2]J. L. Mead, S. Singh, D. K. Roylance, and J. Patt, "Elastomers and Rubber Technology," Eds. R. E. Singler and C. A. Byrne, Library of Congress 86-600600, pp. 251 - 268.

[3]J. L. Mead, and E. R. Pattie, "Elastomers and Rubber Technology," Eds. R. E. Singler and C. A. Byrne, Library of Congress 86-600600, pp. 273 - 280.

[4]G. B. McKenna, G. W. Bullman, K. M. Flynn, and J. Patt, "Elastomers and Rubber Technology," Eds. R. E. Singler and C. A. Byrne, Library of Congress 86-600600, pp. 525 - 534.

[5]"ABAQUS Theory Manual, Version 5.8," Hibbitt, Karlsson & Sorensen Inc., 1080 Main St., Pawtucket, RI, 02860.

[6]I. M. Ward, "Mechanical Properties of Solid Polymers," John Wiley and Sons, 1983.

[7]L. E. Malvern, "Introduction to the Mechanics of a Continuous Medium," Prentice-Hall, 1969.

[8]R. W. Ogden, "Non-Linear Elastic Deformations," Ellis Horwood Limited, 1984.

[9]A. R. Johnson, C. J. Quigley, and J. L. Mead, RUBBER CHEM. TECHNOL., **67**, 904 (1994).

[10]C. J. Quigley, J. L. Mead, and A. R. Johnson, RUBBER CHEM. TECHNOL., **68**, 230 (1995).

[11]R. M. Christensen, "Theory of Viscoelasticity, An Introduction," Academic Press, 1971.

[12]S. A. Hill, NASA TM-108394, February 1993.

[13]T. Chen, NASA TM-2000-210213 (ARL-TR-2206), May 2000.

[14]S. K. Clark and R. N. Dodge, NASA Contractor Report 3629, 1982.

[15]D. R. Pitts and L. E. Sissom, "Heat Transfer," McGraw-Hill Book Co. Library of Congress 77-20255.

APPENDIX

The following notation is included to assist the reader with the description of the ABAQUS finite element algorithm for rubber viscoelasticity.

X_i $(i = 1,2,3)$	coordinates of a material point in the reference configuration.
x_i $(i = 1,2,3)$	coordinates of a material point in the deformed configuration.
$\mathbf{x} = \mathbf{x}(\mathbf{X}, \mathrm{t})$	vector mapping between the reference and deformed configurations.
$\mathbf{F} = \dfrac{\partial \mathbf{x}}{\partial \mathbf{X}}$	deformation gradient.
$J = \det(\mathbf{F})$	determinate of $\mathbf{F}$ which measures volume change.
$\overline{\mathbf{F}} = J^{-\frac{1}{3}}\mathbf{F}$	deformation gradient scaled for volume change.
$\overline{\mathbf{B}} = \overline{\mathbf{F}}\,\overline{\mathbf{F}}^T$	left Cauchy Green strain tensor.
$\bar{I}_1 = tr(\overline{\mathbf{B}})$	first strain invariant (adjusted for volume).
$\bar{I}_2 = \dfrac{1}{2}\left(\left(\bar{I}_1^2\right) - tr(\overline{\mathbf{B}}\,\overline{\mathbf{B}})\right)$	second strain invariant (adjusted for volume).
$\delta\mathbf{u}$	displacement.
$\delta\mathbf{L} = \dfrac{\partial \delta\mathbf{u}}{\partial \mathbf{x}}$	gradient of displacement.
$\delta\mathbf{D} = \dfrac{1}{2}\left(\delta\mathbf{L} + \delta\mathbf{L}^T\right)$	rate of deformation.
$\delta\mathbf{D}_{\mathbf{v}}$	rate of deformation computed using virtual displacement $\delta\mathbf{v}$.
$\mathbf{A} : \mathbf{B}$	scalar product of matrices $\mathbf{A}$ and $\mathbf{B}$.
$\delta\varepsilon^{vol} = \mathbf{I} : \delta\mathbf{D}$	volumetric strain rate.
$\delta\mathbf{e} = \delta\mathbf{D} - \dfrac{1}{3}\delta\varepsilon^{vol}\mathbf{I}$	deviatoric strain rate.
$p = -\dfrac{1}{3}\mathbf{I} : \mathbf{s}$	pressure stress (hydrostatic).

Table I.

Thermal properties.

Property		Rubber	Steel
Conductivity, $J/\left(^{\circ}C\,m\,\mathrm{s}\right)$	$\kappa =$	0.20934	45.83379
Density, kg/m^3	$\rho =$	1000.	7849.
Specific heat, $J/\left(kg\,^{\circ}C\right)$	$c =$	2093.4	460.
Expansion, $\left(^{\circ}C\right)^{-1}$	$a =$	$80.*10^{-6}$	$12.*10^{-6}$

FIGURE CAPTIONS

Figure 1. Axisymmetric CAX8RHT element.

Figure 2. Rubber cylinder, finite element mesh, fixture, and steel disk.

Figure 3. Deformation of a tall uniform cylinder (H = 0.05 m).

Figure 4. Viscoelastic softening of a tall uniform cylinder (H = 0.05 m).

Figure 5. Increase in temperature as a function of time at the center of each uniform cylinder.

Figure 6. Deformation of a tall cylinder with an internal disk (H = 0.05 m).

Figure 7. Temperature distribution in a tall cylinder with an internal disk (H = 0.05 m).

Figure 8. Temperature as a function of time for a tall cylinder with an internal disk (H = 0.05m).

Figure 9. Temperature distribution in a short cylinder with an internal disk (H = 0.0125 m).

Figure 10. Temperature as a function of time for a short cylinder with an internal disk (H = 0.0125 m).

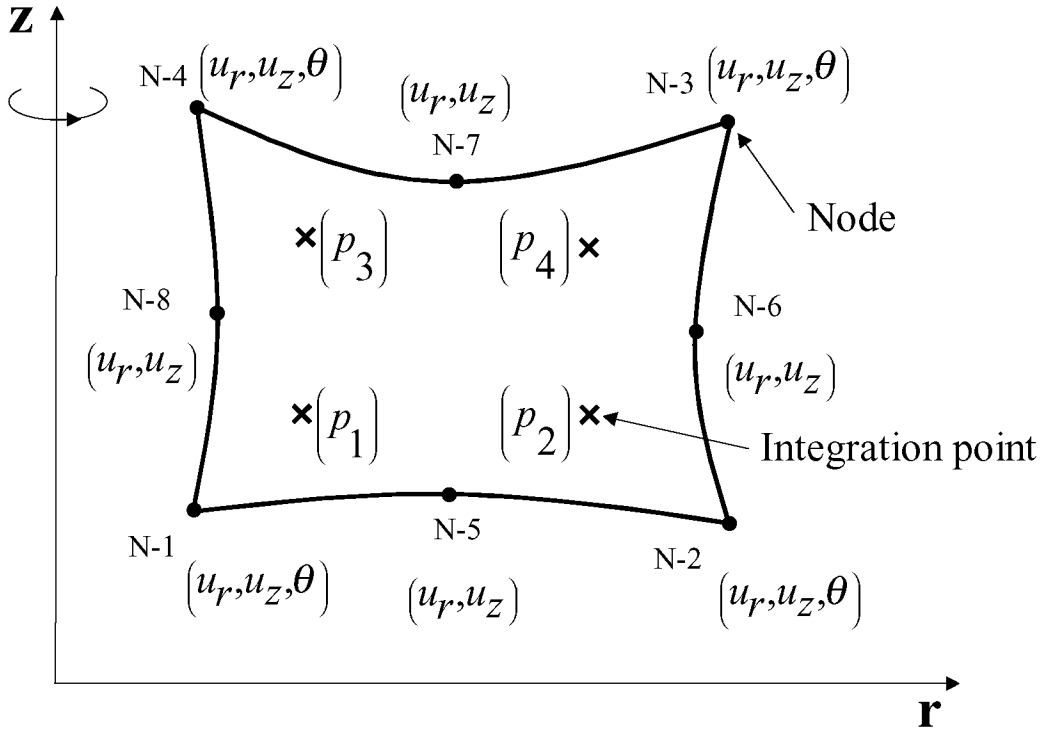

Figure 1. Axisymmetric CAX8RHT element.

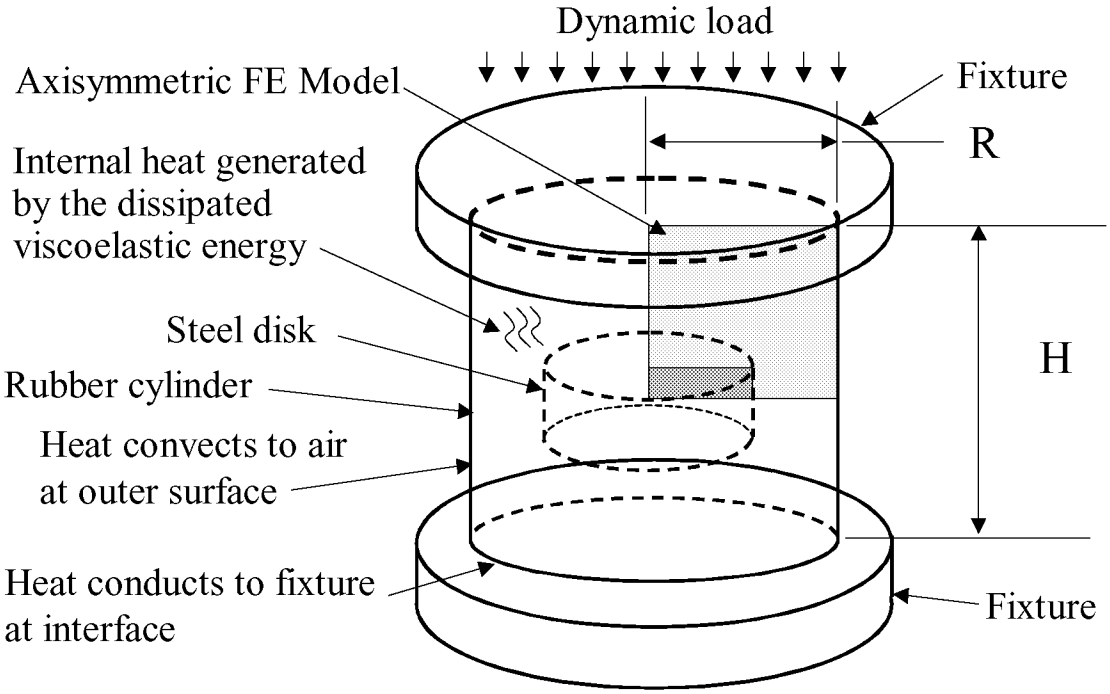

Figure 2. Rubber cylinder, finite element mesh, fixture, and steel disk.

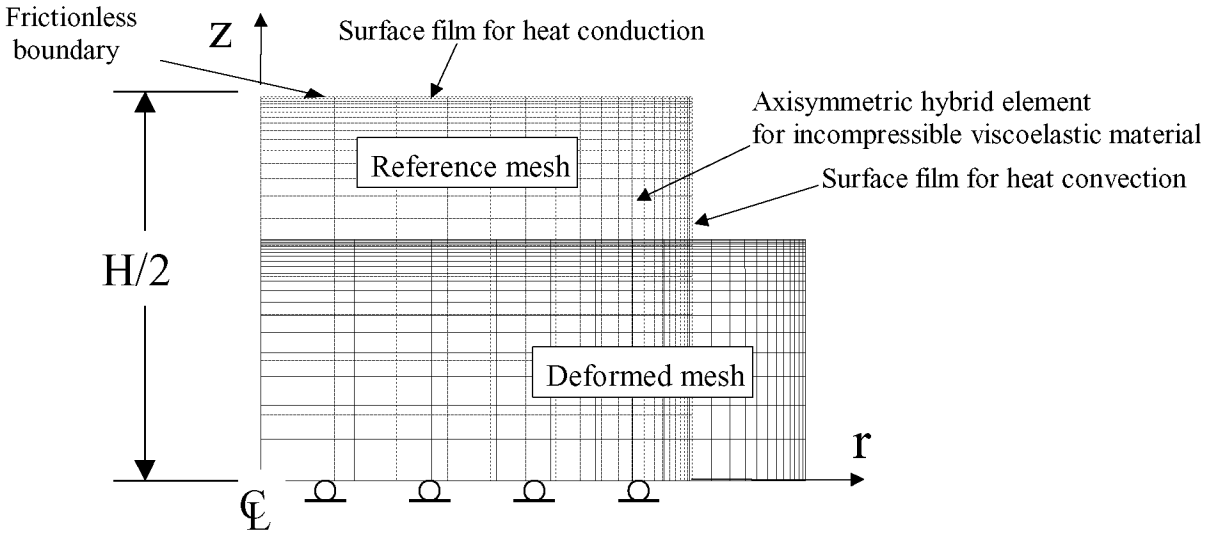

Figure 3. Deformation of a tall uniform cylinder (H = 0.05 m).

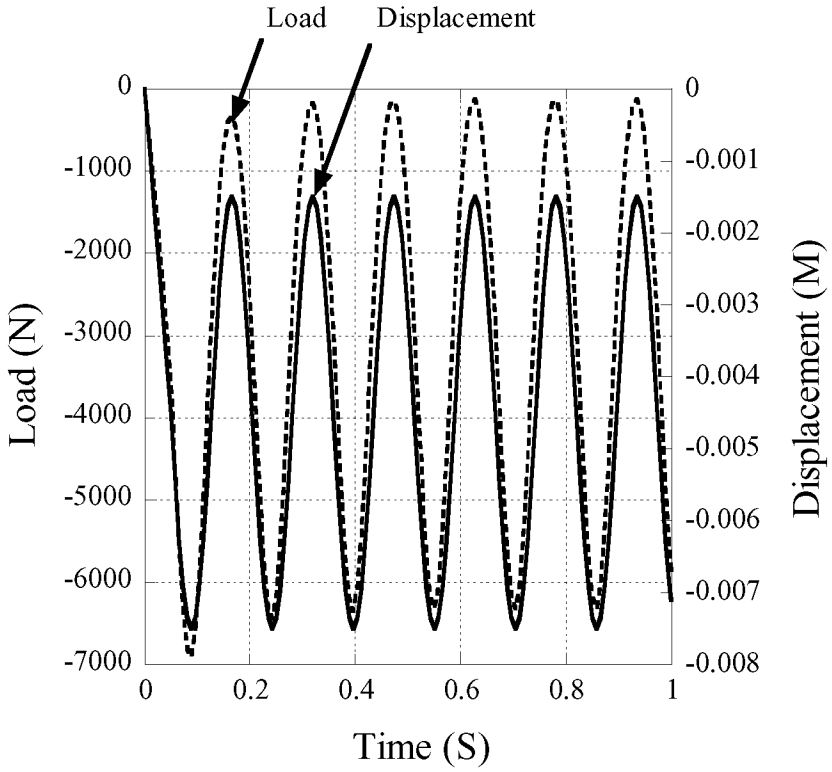

Figure 4. Viscoelastic softening of a tall uniform cylinder (H = 0.05 m).

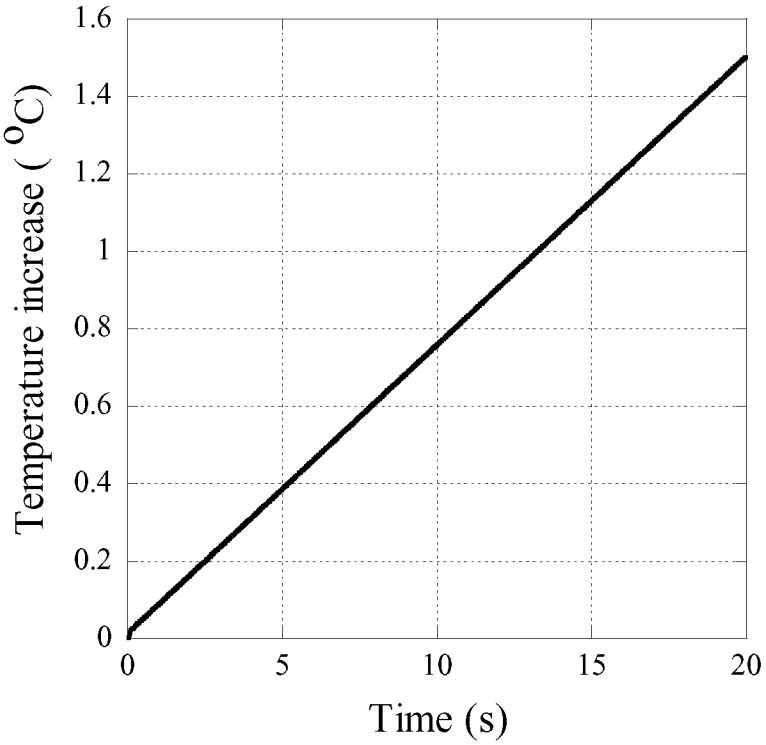

Figure 5. Increase in temperature as a function of time at the center of each uniform cylinder.

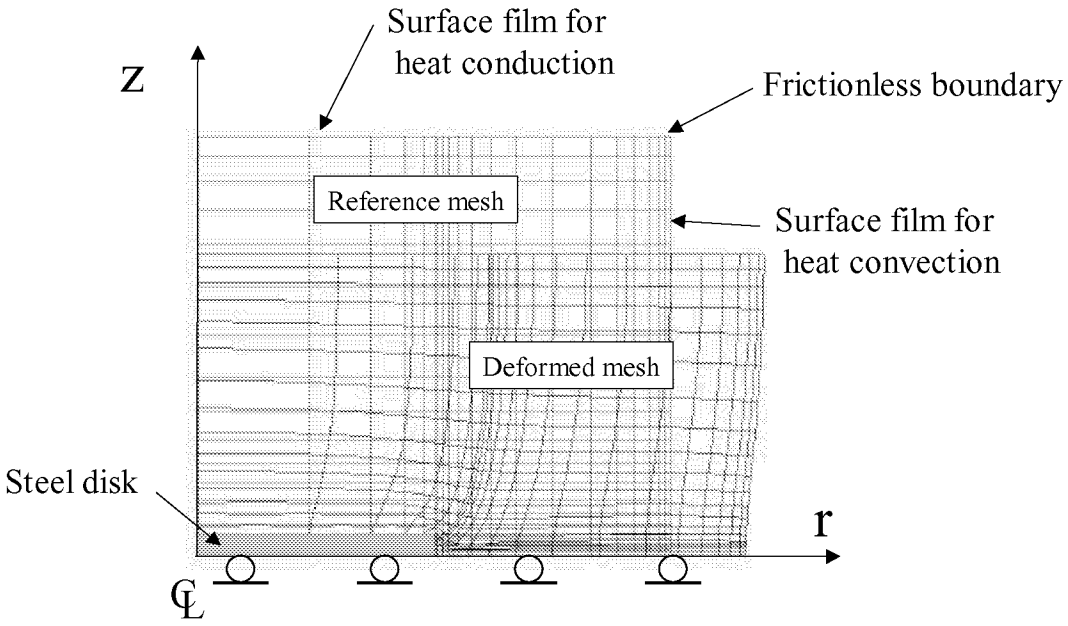

Figure 6. Deformation of a tall cylinder with an internal disk (H = 0.05 m).

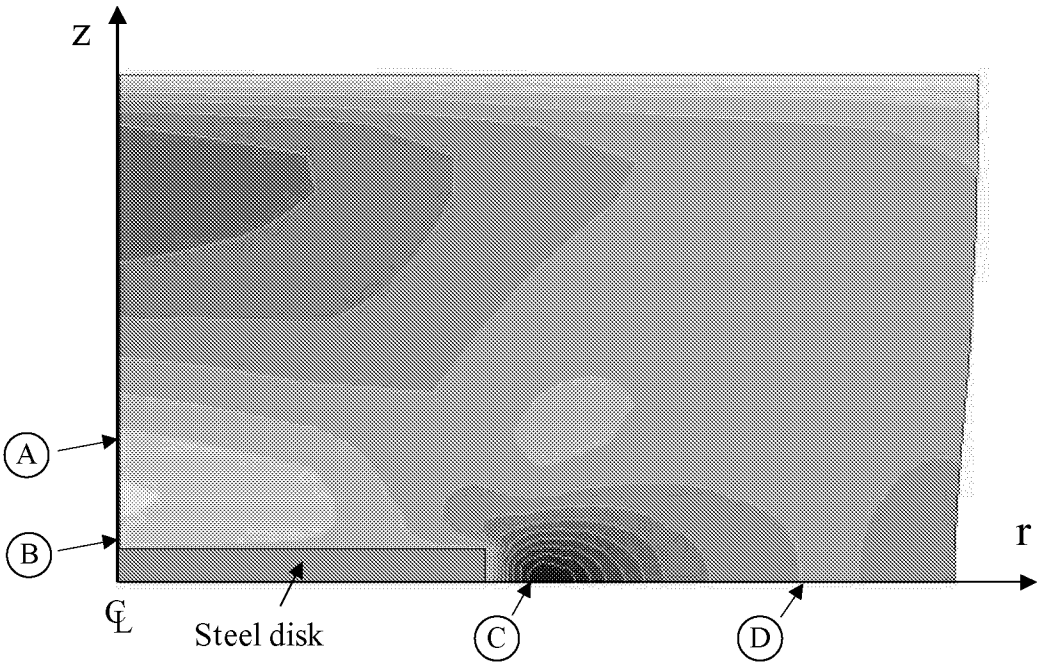

Figure 7. Temperature distribution in a tall cylinder with an internal disk (H = 0.05 m).

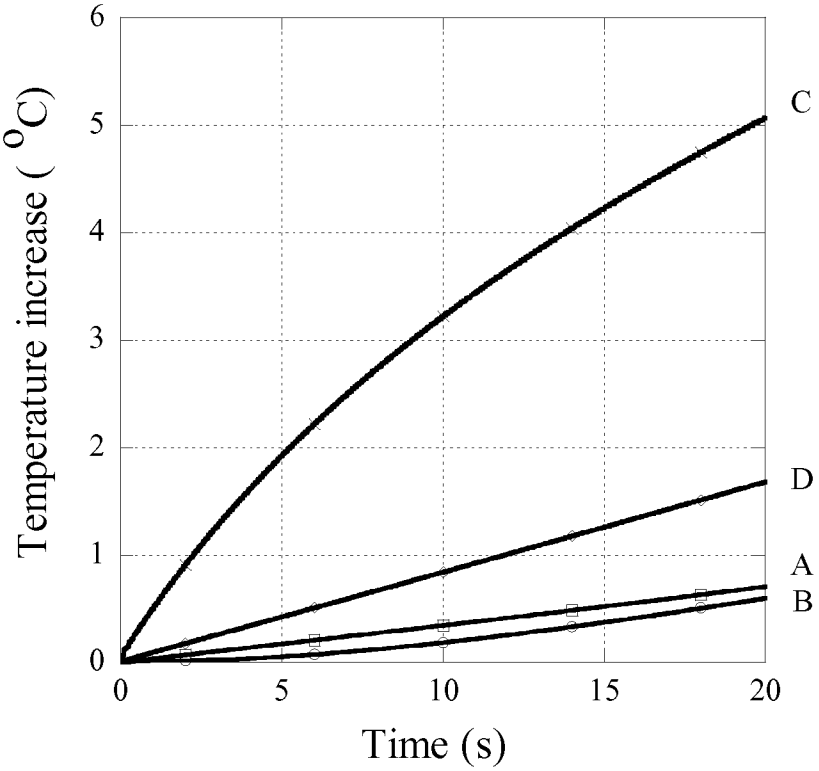

Figure 8. Temperature as a function of time for a tall cylinder with an internal disk (H = 0.05m).

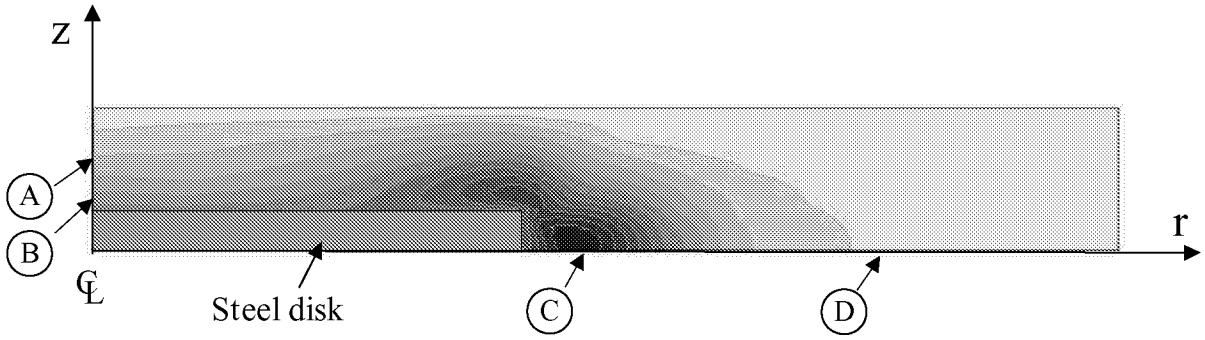

Figure 9. Temperature distribution in a short cylinder with an internal disk (H = 0.0125 m).

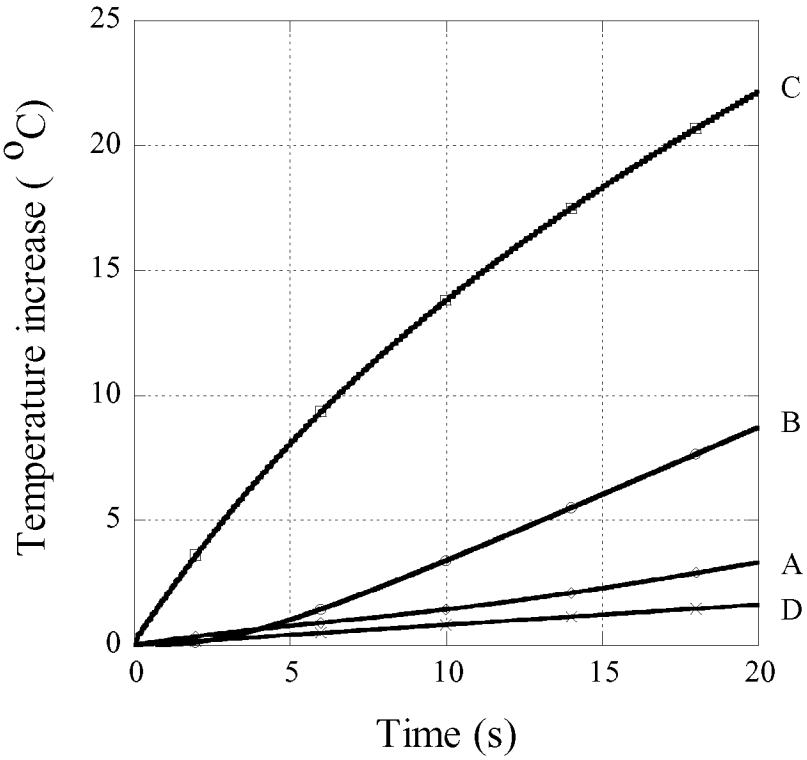

Figure 10. Temperature as a function of time for a short cylinder with an internal disk (H = 0.0125 m